Nanoscale

Cite this: *Nanoscale*, 2012, **4**, 6025

www.rsc.org/nanoscale

PAPER

Amperometric biosensor based on 3D ordered freestanding porous Pt nanowire array electrode†

Yunli Wang,[a] Yingchun Zhu,*[a] Jingjing Chen[b] and Yi Zeng[b]

Received 22nd May 2012, Accepted 17th July 2012
DOI: 10.1039/c2nr31256e

A three-dimensionally (3D) ordered freestanding porous platinum (Pt) nanowire array electrode (PPNWAE) with pores of several nanometers in size and a Pt nanowire array electrode (PNWAE) without pores were facilely fabricated by metal electrodeposition and direct integration with a Pt disk electrode. The unusual PPNWAE with high active area showed excellent sensitivity (0.36 mA cm^{-2} mM^{-1}) and a wide detection range (4.5 μM–27.1 mM) to hydrogen peroxide (H_2O_2). A glucose oxidase (GOD)-based biosensor (PPNWAE/GOD) with a considerably wide detection range (4.5 μM–189.5 mM) to glucose was demonstrated. Furthermore, a lower detection limit, higher sensitivity and smaller value of Michaelis–Menten constant k_m were recorded for PPNWAE-based biosensors compared with PNWAE-based biosensors. Particularly, the response current to glucose of PPNWAE/GOD was *ca.* 100% higher than that of PNWAE/GOD and the response current to H_2O_2 of PPNWAE was *ca.* 50% higher than that of PNWAE, owing to the granular and rougher porous nanowire surface enabling greater bioactivity for GOD. The selectivity of PPNWAE/GOD glucose biosensor was also estimated.

1. Introduction

For a long time, fast and accurate determination of glucose has been a vital subject as glucose concentration is a crucial indicator for many diseases, such as diabetes and endocrine metabolic disorders.[1] Recently, reliable glucose biosensors have been developed by using electrochemical,[2] chemiluminescence[3] and other methods.[4] Among these methods, glucose biosensors based on electrochemistry, especially amperometric biosensors employing glucose oxidase (GOD), have drawn much attention due to their merits of simplicity, high selectivity and relatively low cost.[5–7] The employed enzyme GOD catalytically converts glucose into gluconic acid accompanied by generation of hydrogen peroxide (H_2O_2) to which the amount of glucose is proportional.[8] It was well recognized that the performance of such glucose biosensors strongly relied on the electrode materials. Therefore, it is highly desirable to search for materials sensitive to H_2O_2 that in addition are capable of providing a good environment for efficient enzyme loading and maintenance of enzyme bioactivity.

As important one-dimensional (1D) nanostructures, nanowires possess a high surface area-to-volume ratio, rendering them extremely sensitive to species adsorbed on their surfaces and resulting in excellent sensitivity and activity.[9–11] The most common assembly of nanowires is known as a nanowire array. This ordered electrode structure with high surface area has been widely used to assemble sensors[12] because it can enhance the electrochemical properties and electrocatalytic activity.[13–15] As is well known, the noble metal Pt can strongly catalyze the decomposition of H_2O_2 into water and oxygen.[16] Moreover, with the aforesaid advantages, Pt nanowire array electrodes with a high electrochemically active area have been applied in sensors.[17–19] The current response to H_2O_2 at Pt electrode was under mixed kinetic and diffusion control and further complicated by competitive adsorption of oxygen onto Pt active surface sites and the protonation of the adsorbed H_2O_2 complex species.[20] The faradic currents associated with the kinetically controlled electrochemical events were sensitive to the nanoscopic active surface area.[21] High surface area mesoporous Pt microelectrodes have also been used for H_2O_2 detection and raising the upper detection limit.[22] One valid strategy could be adopted to boost further the active sites of nanowire array electrodes by introducing pores for each nanowire element. In other words, a three-dimensionally (3D) ordered porous nanowire array may enhance activity dramatically.

Little work has been done on electrochemical sensors for H_2O_2 and glucose utilizing 3D ordered freestanding porous Pt nanowire array electrodes (PPNWAE), despite a report in which a porous Pt nanowire array was pasted onto the electrode of an ethanol fuel cell.[23] In this work, we fabricated such PPNWAE by co-electrodepositing Pt–Cu nanowires into the porous

[a]*State Key Laboratory of High Performance Ceramics and Superfine Microstructure, Key Lab of Inorganic Coating Materials, Shanghai Institute of Ceramics, Chinese Academy of Sciences, Shanghai 200050, China. E-mail: yzhu@mail.sic.ac.cn; Fax: +86-21-52412632; Tel: +86-21-52412632*
[b]*Analysis and Testing Center for Inorganic Materials, Shanghai Institute of Ceramics, Chinese Academy of Sciences, Shanghai 200050, China*
† Electronic supplementary information (ESI) available. See DOI: 10.1039/c2nr31256e

track-etched polycarbonate template membrane and preferentially de-alloying the Cu component.[24] Distinct from other nanowire array electrodes, we integrated the substrate Pt disk electrode and the nanowire array by direct growth of nanowires onto a Pt disk electrode according to our former work,[25] which makes the prepared electrode more stable and more conductive in solution than methods that fix the array onto the substrate electrode with binders.[9,26] The electrochemical performance was studied with H_2O_2 and glucose as targets. The PPNWAE and GOD modified PPNWAE biosensor (PPNWAE/GOD) showed considerably wide detection ranges toward H_2O_2 and glucose with good sensitivities and low detection limits. To highlight the synergistic effect of the porous nanostructure and the anowire array structure, a Pt nanowire array electrode (PNWAE) was also prepared and anaylsed. The results showed clearly that PPNWAE behaved better than PNWAE.

2. Experimental

2.1. Reagents

The porous track-etched polycarbonate membrane (PC membrane, pore diameter: 400 nm, pore density: 1.2×10^8 cm^{-2}, thickness: 10 μm) was purchased from Whatman (USA). Boric acid (H_3BO_3, 99.5%), copper nitrate ($Cu(NO_3)_2 \cdot 3H_2O$, 99%), hexachloroplatinic acid ($H_2PtCl_6 \cdot 6H_2O$, 37%), nitric acid (HNO_3, 68%), dichloromethane (CH_2Cl_2, 99.5%), potassium hexacyanoferrate(III) ($K_3Fe(CN)_6$, 99.5%), potassium hexacyanoferrate(II) trihydrate ($K_4Fe(CN)_6 \cdot 3H_2O$, 99.5%), glutaraldehyde (GA, 50%), hydrogen peroxide (H_2O_2, 30%), D-(+)-glucose (99.5%), ascorbic acid (AA, 99.7%) and uric acid (UA, 99%) were all obtained from Sinopharm Chemical Reagent Co., Ltd., China. Glucose oxidase from *Aspergillus niger* (GOD, EC 1.1.3.4, 10 KU) was provided by Sigma-Aldrich Co. LLC. 0.553 M standard H_2O_2 solution, which was standardized by $KMnO_4$ standard solution, was freshly prepared by diluting 30% H_2O_2 with double-distilled water. The standard H_2O_2 solutions of lower concentrations were obtained by diluting 0.553 M standard H_2O_2. A 0.1 M phosphate buffer solution (PBS, pH 7.0) containing 0.1 M KCl was used as supporting electrolyte during electrochemical measurements. The other chemicals were analytical reagents and all solutions employed were prepared from double-distilled water.

2.2. Preparation of PPNWAE

The steps to fabricate PPNWAE are presented in detail as follows. Firstly, the porous polycarbonate membrane used as template was fixed on the surface of Pt disk electrode with a Teflon cap as shown in Fig. S1 (ESI†). The Pt–Cu alloy nanowires were galvanostatically deposited at −60 μA into the pores with a solution of 50 mM H_3BO_3 containing 5 mM H_2PtCl_6 and 15 mM $Cu(NO_3)_2$. The template was then dissolved in CH_2Cl_2 to release the nanowire array. At last, the Pt–Cu alloy nanowire array was dealloyed in 25% HNO_3 to remove the Cu component so as to form a 3D-ordered, freestanding, porous Pt nanowire array. The obtained array was washed with double-distilled water and ethanol for further use. The fabrication procedure of PNWAE was the same as that of PPNWAE, except the electroplating solution contained only 50 mM H_3BO_3 and 5 mM H_2PtCl_6.

2.3. Immobilization of GOD

Initially, PPNWAE was electrochemically cleaned by cyclic voltammetry in 0.5 M H_2SO_4 and thoroughly cleaned with double-distilled water and PBS. GOD was immobilized on PPNWAE with the glutaraldehyde cross-linkage method. At first, 15 μL GOD (5 KU mL^{-1}) and 7.5 μL glutaraldehyde (wt 5%) were mixed adequately. Then 10 μL of this intermixture was spread onto the surface of the electrode and cross-linked at 4 °C for 12 h. Then, the modified electrode (PPNWAE/GOD) was rinsed with double-distilled water and PBS in order to remove unfixed molecules for electrochemical testing. PNWAE was also modified in the same way to get PNWAE/GOD.

2.4. Measurements

A conventional three-electrode system was employed in all measurements, where PPNWAE, PNWAE, PPNWAE/GOD or PNWAE/GOD served as the working electrode, Ag/AgCl electrode with a saturated KCl internal solution served as the reference electrode and a spiral Pt wire acted as the counter electrode. The CV and amperometric response measurements were performed on a Solartron Electrochemical Interface (model 1287), while electrochemical impedance spectroscopy (EIS) measurements were carried out on a Solartron Impedance/Gain-Phase Analyzer (model 1260). PPNWAE, PNWAE and Pt disk electrode (PE) were electrochemically treated by cyclic voltammetry (CV) in 0.5 M H_2SO_4 before measurements. CV curves of PPNWAE, PNWAE and PE in 0.5 M H_2SO_4 as well as PPNWAE in PBS containing $K_3Fe(CN)_6/K_4Fe(CN)_6$ were recorded. Amperometric response measurements of H_2O_2 and glucose were carried out at 0.55 V, the potential at which amperometric enzyme sensors are usually operated to detect the enzymatic product H_2O_2. In EIS experiments, the dc potential, potential amplitude of the ac signal and frequency range were set as 0.25 V, 10 mV and 10^{-1} to 10^6 Hz, respectively. All measurements were carried out at 25 °C.

3. Results and discussion

3.1. Characterization of PPNWAE

Fig. 1A shows a top-view SEM image of the prepared freestanding porous Pt nanowire array. It was found the obtained porous Pt nanowire array was stable and orderly since a relatively low plating current was adopted.[23] It also could be seen that, for most of the nanowires, the spacing between two nanowires was larger than diameter of the nanowires. This larger spacing made the deposited porous Pt nanowires more disperse and independent, compared with the nanowire clusters prepared from anodic aluminium oxide (AAO) templates.[26–28] As far as slow heterogeneous kinetics, such as H_2O_2 oxidation and glucose oxidation on the electrode, were concerned, the local diffusion rate was elevated and each freestanding porous Pt nanowire behaved more like an individual nanoelectrode; thus the response current increased concomitantly.[10,17,29]

Both the end parts and central parts of the Pt nanowires appeared porous, with small nanopores of several nanometers, as shown in TEM images of the side edge of a porous Pt nanowire (Fig. 1B and C). This meant that the porous Pt nanowire array

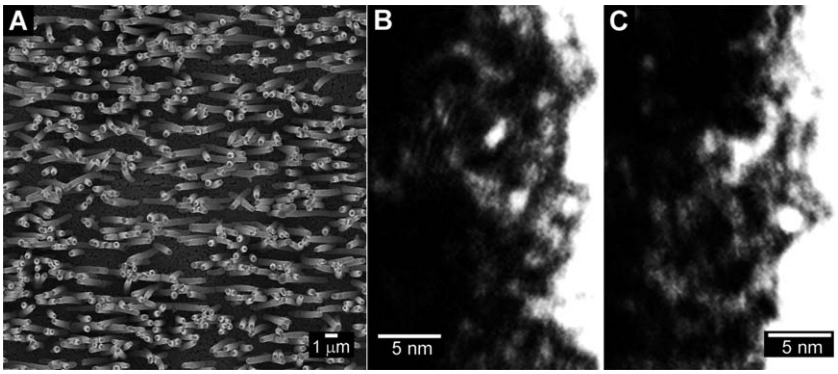

Fig. 1 (A) Top-view SEM image of the fabricated 3D ordered freestanding porous Pt nanowire array electrode (PPNWAE). TEM images: (B) lateral edge of central part of porous Pt nanowire and (C) lateral edge of end part of porous Pt nanowire.

integrated with the substrate Pt electrode had a good combination of stability and porosity. In addition, this structure was in favor of mass transportation, which was preferential in amperometric biosensor.

3.2. Cyclic voltammetry (CV) properties of PPNWAE

PPNWAE was electrochemically characterized in 0.5 M H_2SO_4 at a scan rate of 100 mV s^{-1} as shown in Fig. 2. For comparison, the CV curves of PNWAE and a bare Pt disk electrode (PE) are also presented as Fig. 2b and c, respectively. Hydrogen adsorption started at about 0.1 V, exhibiting two adsorption peaks (H_{C1} and H_{C2} in Fig. 2). The adsorbed hydrogen was then electrochemically oxidized in the positive potential sweep. By carrying out the integration of the current–time curve from about 0.15 V to −0.1 V, the amount of charge required to deposit hydrogen atoms could be obtained after correction for double-layer charging. The double-layer charging current was assumed to be approximately constant and equal to the current measured at the minimum (about 0.12 V in Fig. 2) of the double-layer charging region. Assuming that the formation of a monolayer of hydrogen required about 120 μC cm^{-2} of real surface area,[30] the true surface area of PPNWAE and PWNAE were evaluated to be 10.08 cm^2 and 3.5 cm^2, respectively. The roughness factor (R_f) of PPNWAE was calculated to be 144 while that of PNWAE was 50, whereas the geometric area of PE was 0.07 cm^2. The 3D ordered porous nanowire array structure enabled PPNWAE to have a much larger area than its apparent geometric area and than PNWAE, which facilitates efficient mass transport and electron transfer for applications in biosensor.

The CV curves of PPNWAE in 0.1 M PBS containing 0.01 M $K_3Fe(CN)_6$–$K_4Fe(CN)_6$ and 0.1 M KCl at different scan rates from −0.2 V to 0.6 V were shown in Fig. 3A. The symmetrical anodic and cathodic peaks associated with oxidation of $K_4Fe(CN)_6$ and reduction of $K_3Fe(CN)_6$ could be observed at any scan rate on PPNWAE. The separations between the anodic and the cathodic peak potentials varied slightly with the increase of scan rate, showing 64.83 mV at 10 mV s^{-1}, 74.65 mV at 20 mV s^{-1}, 78.29 mV at 40 mV s^{-1}, 68.23 mV at 60 mV s^{-1}, 72.73 mV at 80 mV s^{-1} and 70.87 mV at 100 mV s^{-1}, respectively. Additionally, the ratios of anodic/cathodic peak currents approached 1 while the anodic peak currents (I_P) depended linearly on square root of the scan rates ($v^{1/2}$), as shown in Fig. 3B, indicating that both ferrocyanide and ferricyanide presented reversibility during the electrode process and that transformation between $K_3Fe(CN)_6$ and $K_4Fe(CN)_6$ on the surface of PPNWAE was diffusion controlled. These facts might show that charge transfer occurred rapidly on such PPNWAE.

3.3. Detection of H_2O_2 with PPNWAE

It is well known that Pt as a noble metal shows excellent electrocatalytic activity. Furthermore, PPNWAE displayed unique electrical properties based on its special structure. Here,

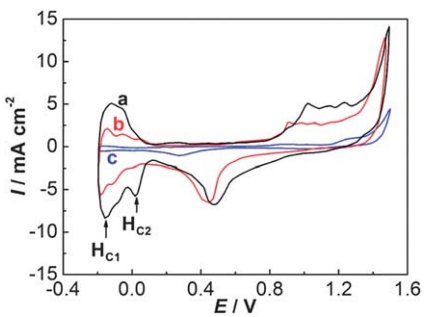

Fig. 2 CV curves in 0.5 M H_2SO_4 at the scan rate of 100 mV s^{-1}: (a) 3D ordered freestanding porous Pt nanowire array electrode (PPNWAE), (b) Pt nanowire array electrode (PNWAE) and (c) bare Pt disk electrode (PE).

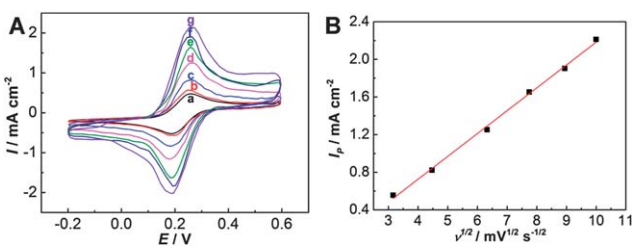

Fig. 3 (A) CV curves in 0.1 M PBS containing 10 mM $K_3Fe(CN)_6$–$K_4Fe(CN)_6$ and 0.1 M KCl: (a) glucose oxidase modified porous Pt nanowire array electrode (PPNWAE/GOD), (b)–(g) PPNWAE. a, b 10 mV s^{-1}, c 20 mV s^{-1}, d 40 mV s^{-1}, e 60 mV s^{-1}, f 80 mV s^{-1}, g 100 mV s^{-1}. (B) Relationship between anodic peak current and square root of the scan rate in (A).

PPNWAE was examined for its amperometric response toward H_2O_2. Fig. 4A(a) depicted the typical amperometric response of PPNWAE to H_2O_2 oxidation by successive addition of certain concentrations of H_2O_2. A fast and sensitive response was observed with changes in level of H_2O_2, achieving a steady signal within 5 s. A detection limit of 3.6 μM was obtained. The low detection limit may result from the advantages of the nanowire array in improving the S/N ratio. The amperometric response of PNWAE to H_2O_2 was also presented in Fig. 4A(b). It could be seen that the response of PNWAE was less sensitive than that of PPNWAE, especially at the initial stage of H_2O_2 injection. PNWAE didn't give an obvious response until addition of 553 μM H_2O_2. The outstanding performance for PPNWAE could be ascribed to the porous structure which could improve the active surface area tremendously.

Based on the amperometric responses, the calibration curves were obtained in Fig. 4B. The amperometric signal increased with the rise of H_2O_2 concentration and the relation for PPNWAE could be expressed as

$$I = 8.43324 + 364.2805C_{H_2O_2}, (C_{H_2O_2} = 4.5\ \mu M–0.43\ mM, R = 0.9998) \quad (1)$$

$$I = 0.00152 + 0.25638C_{H_2O_2} - 0.0038C^2_{H_2O_2}, (C_{H_2O_2} = 0.43\ mM –27.1\ mM, R = 0.9985) \quad (2)$$

As described above, in the H_2O_2 concentration range of 4.5 μM–0.43 mM, the amperometric signal was linearly related to the H_2O_2 concentration with sensitivity of 0.36 mA cm^{-2} mM^{-1}, 2.4 times higher than that of PNWAE. In higher H_2O_2 concentration range until 27.1 mM, the amperometric signal and H_2O_2 concentration had the relation as shown in eqn (2) with a sensitivity of *ca.* 0.26 mA cm^{-2} mM^{-1} while the sensitivity of PNWAE was *ca.* 0.18 mA cm^{-2} mM^{-1}. The sensitivities of both electrodes were much superior to the reported 0.096 mA cm^{-2} mM^{-1} with Pt nanowires,[31] 0.07 mA cm^{-2} mM^{-1} with horseradish peroxidase,[32] and 0.01 mA cm^{-2} mM^{-1} with a conventional Pt electrode,[33] indicating that PPNWAE exhibited excellent electrocatalytic activity toward H_2O_2 due to its higher active area. The whole detection range was 4.5 μM–27.1 mM, covering 4 orders of magnitude. This obtained detection range was comparable to the sensor utilizing synergic action of carbon nanotubes and Pt nanowires (1 μM–30 mM)[34] and wider than the biosensor based on myoglobin/gold nanoparticles/carbon spheres 3D architecture bioconjunction (0.28 μM–0.84 mM).[35]

3.4. Electrochemical properties of PPNWAE/GOD

As an effective method for examining the electrode–solution interfacial properties, especially those with modified surfaces, electrochemical impedance spectroscopy (EIS) was employed to investigate the nature of PPNWAE and effect of GOD modification on the electron transfer kinetics at electrode surface as shown in Fig. 5. The experimental impedance spectroscopies were fitted according to a traditional Randles electrical circuit (Fig. 5, top inset). This circuit included the ohmic resistance of the electrolyte solution (R_s), the interfacial charge transfer resistance (R_{ct}) corresponding to the redox probe charge transfer process, the Warburg impedance (W) resulting from diffusion of ions from bulk electrolyte to electrode and the double layer capacitance (CPE). A CPE (constant phase element) instead of pure capacitance was used to describe the double layer capacitance in view of the electrodes' roughness and porosity.[36,37] The impedance of a CPE was represented by[38,39]

$$Z = 1/[T(i\omega)^P] \quad (3)$$

where i is an imaginary number, ω is the angular frequency, T (CPE-T) is the admittance constant, P (CPE-P) is an adjustment

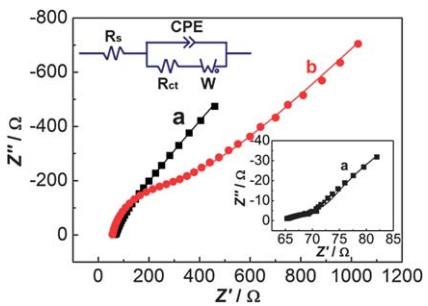

Fig. 5 Experimental (scattered line) and fitted (solid line) Nyquist plots of EIS in 0.1 M PBS containing 10 mM $K_3Fe(CN)_6$–$K_4Fe(CN)_6$ and 0.1 M KCl: (a) porous Pt nanowire array electrode (PPNWAE) and (b) glucose oxidase modified PPNWAE (PPNWAE/GOD). The top inset was equivalent circuit used to fit EIS. The bottom inset was the EIS curve of PPNWAE at high frequencies.

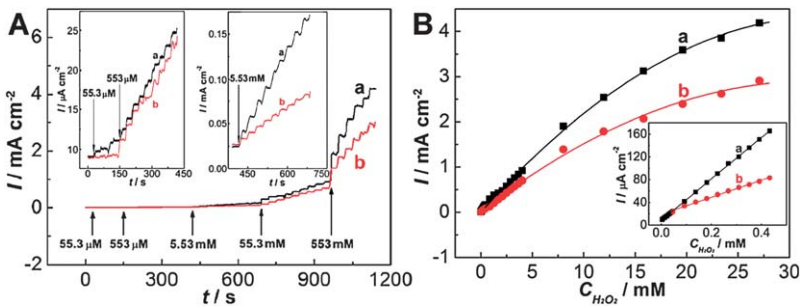

Fig. 4 (A) Amperometric response with successive addition of certain concentrations of H_2O_2 to stirred 0.1 M PBS at 0.55 V: (a) porous Pt nanowire array electrode (PPNWAE) and (b) Pt nanowire array electrode (PNWAE). The insets are current–time curves upon addition of lower concentrations of H_2O_2. (B) Calibration curves according to (A): (a) PPNWAE and (b) PNWAE. The inset presents the calibration curves for lower concentrations of H_2O_2.

parameter ($0 \leq P \leq 1$). P is related to the phase angle α by $\alpha = (1 - P)90°$. For a perfect capacitor, $\alpha = 0$, $P = 1$ and T is the capacitance. In the limiting case of $P = 0$, the impedance represents a resistor. When values of P are between 0 and 1, the P value reflects directly the roughness of the electrode. Hence, from the fitting parameter values listed in Table 1, it could be seen that the very small P value of PPNWAE indicated a fairly rough and porous surface. In general, the quite rough and porous structured electrode would effectively accelerate electrolyte diffusion and electron transfer, which was advantageous for biosensors.[40] Assuming the electrode–solution interface behaved like a parallel-plate capacitor, GOD modification smoothed the surface to a certain extent resulting in a rising P value, accompanied by a diminishing electrode area leading to decrease of T according to[41]

$$C = \varepsilon\varepsilon_0 S/d \quad (4)$$

where C is the capacitance, ε is the dielectric constant, ε_0 is the permittivity of free space, S is the area of a parallel plate and d is the separation between two plates. After PPNWAE was functionalized with GOD, the electron transfer between the electrochemical probe and electrode surface was inhibited, owing to the GOD insulator layer and the electrostatic repulsion of GOD (PI: 4.2) with negative charges and the negatively charged electrochemical probe. This brought the elevation in R_{ct} and fall in peak current as shown in Fig. 3A(a). The modified film might partly obstruct the diffusion of redox probe from solution to electrode, showing an increased W value.

3.5. Detection of glucose with PPNWAE/GOD

As studied above, PPNWAE exhibited prominent electrocatalytic activity toward H_2O_2, which meant the electrode could serve as an ideal electrochemical platform for constructing oxidase-based biosensors. With glucose oxidase as a model enzyme, a glucose biosensor was fabricated *via* cross-linkage to immobilize enzyme as presented in Fig. 6A. The reactions involved in glucose detection were depicted in Fig. 6B. Under air-saturated conditions, glucose molecules (Glc) diffused from the analyte solution to the electrode surface and reacted with flavin adenine dinucleotide, the active center of GOD, leading to the conversion of glucose into gluconic acid and the oxidized form of GOD ($GOD_{(Ox)}$) into the reduced form ($GOD_{(Red)}$). $GOD_{(Red)}$ was then oxidized rapidly to $GOD_{(Ox)}$ again by dissolved oxygen in water, accompanied by formation of H_2O_2. The amount of glucose could be examined by measuring the anodic oxidation current of the produced H_2O_2.[42]

Fig. 7A shows a fast and sensitive amperometric response toward glucose with a steady-state current achieved in 4–10 s. Meanwhile, the detection limit of PPNWAE/GOD glucose biosensor was determined to be 4.5 μM. However, PNWAE/GOD could not respond noticeably until 5 mM glucose was added. The amperometric signal of PPNWAE/GOD increased with the increase of glucose concentration, as shown in the calibration curve (Fig. 7B(a)), and the relation could be expressed as

$$I = 0.61763 - 0.40723\exp(-C_{Glc}/204.97586) - 0.2055\exp(-C_{Glc}/11.73513),\ (R = 0.9999) \quad (5)$$

Table 1 Fitting parameters based on equivalent electrical circuit shown in the top inset of Fig. 5 for different EIS plots

Electrodes	CPE-T/μF	CPE-P	R_{ct}/Ω	W/Ω
PPNWAE	1813.20	0.5015	2.77	35.29
PPNWAE/GOD	94.76	0.8665	289	96.7

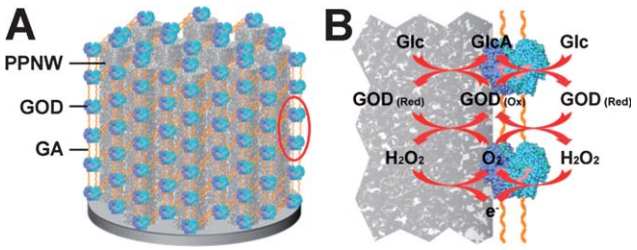

Fig. 6 (A) Pictorial representation of glucose oxidase (GOD) immobilization and (B) biochemical reactions involved in glucose sensing from selected area in (A).

As presented above, in glucose concentration range of 4.5 μM–27.8 mM, the sensitivity was *ca.* 8.74 μA cm^{-2} mM^{-1}, which was more than 2 times higher than that of PNWAE/GOD. The whole detection range was demonstrated to be from 4.5 μM to 189.5 mM, covering 5 orders of magnitudes and much wider than some electrochemical glucose biosensors as listed in Table 2.[17,21,34,40,43–45] The enhancement could be ascribed to the fact that the perpendicularly orientated porous nanowire array provided a large quantity of surface electroactive sites, and thus circumvented the problems related to the limited number of active sites and expanded the upper detection limit.[46] This detection range was sufficient for medical use, for example, in monitoring human blood glucose levels, where the blood glucose concentration in normal human ranges from 4.4 mM to 6.6 mM and in people with diabetes exceeds 11.1 mM.[47] Such a wide detection range opens the opportunity to be applied in the medicine field and the food industry.

In glucose concentration range of 4.5 μM–100 mM, the apparent Michaelis–Menten constant k_m, which depicted the enzyme–substrate kinetics, could be calculated from the evolved Lineweaver–Burk equation:[48]

$$I_s^{-1} = k_m I_{max}^{-1} C_{Glc}^{-1} + I_{max}^{-1} \quad (6)$$

where I_s is the steady-state current, I_{max} is the maximum current measured under substrate saturation and C_{Glc} is the concentration of the substrate, glucose. The k_m values of GOD confined at the surface of PPNWAE and PNWAE were estimated to be 14.6 mM and 17.6 mM, respectively. These values were lower than some recently reported glucose sensors based on a sol–gel/chitosan composite (21 mM),[49] ZnO:Co nanoclusters (21 mM),[50] nano-$CaCO_3$ (21.4 mM),[51] polypyrrole films (37.6 mM).[52] In particular, k_m of GOD in solution was 33–100 mM.[53] The lower k_m suggested a higher enzymatic activity of the immobilized GOD. Thus, the above result further indicated that the PPNWAE/GOD biosensor possesses a high affinity to glucose.

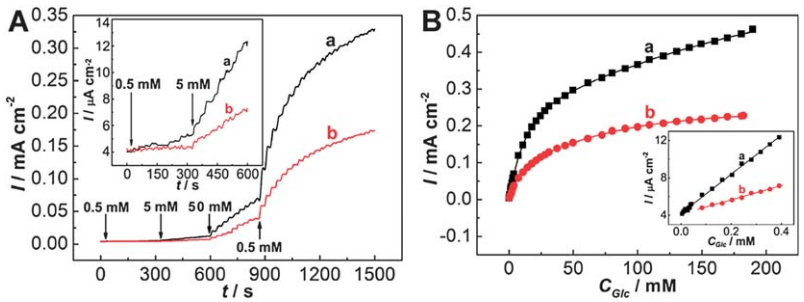

Fig. 7 (A) Amperometric response with successive addition of certain concentrations of glucose to stirred 0.1 M PBS at 0.55 V: (a) glucose oxidase modified porous Pt nanowire array electrode (PPNWAE/GOD) and (b) glucose oxidase modified Pt nanowire array electrode (PNWAE/GOD). The inset shows current–time curves for addition of lower concentrations of glucose. (B) Calibration curves according to (A): (a) PPNWAE/GOD and (b) PNWAE/GOD. The inset depicts the calibration curves for lower concentrations of glucose.

Remarkably, from the results of our research, utilizing PPNWAE instead of PNWAE to test H_2O_2 and glucose could achieve better performance, such as a lower detection limit, a greater sensitivity and a smaller k_m value. In essence, the detection of glucose was directly correlated to H_2O_2 detection; the ratio of the amperometric response to glucose of PPNWAE/GOD to that of PNWAE/GOD should be the same as that of the amperometric response to H_2O_2 of PPNWAE to that of PNWAE. However, at higher concentrations, the response of PPNWAE/GOD was *ca.* 100% higher than that of PNWAE/GOD while the response of PPNWAE was *ca.* 50% higher than that of PNWAE. At lower concentrations, the contrast was more evident. The results may arguably be explained by two aspects. Firstly, because of the porous structure of each nanowire as shown in Fig. 1B and C, the H_2O_2 derived during oxidation of glucose can be electrooxidized on larger active area at PPNWAE. PPNWAE/GOD was more sensitive than PNWAE/GOD to glucose, consistent with the fact that PPNWAE performed better than PNWAE toward H_2O_2. Secondly, the response ratio of PPNWAE/GOD to PNWAE/GOD was mismatched with that of PPNWAE to PNWAE, which could be attributed to the immobilized GOD. Here, with the size of $7 \times 5.5 \times 8$ nm,[54] GOD was unlikely to enter predominately into the pores because most of the pores were not big enough, as shown in Fig. 1B and C. Nevertheless, the side surface of the porous Pt nanowire was granular and rougher while that of normal Pt nanowire was relatively smoother, which would help the immobilization of GOD and facilitate GOD adjusting its conformation so as to better fit substrate molecules,[55] thus improving the production of H_2O_2. This explained why PPNWAE/GOD had a lower k_m value as well.

In order to evaluate the selectivity of PPNWAE/GOD, a test was carried out in the presence of 5.6 mM glucose and interference substances, 0.1 mM ascorbic acid (AA) and 0.02 mM uric acid (UA). The current responses to AA and UA were *ca.* 24% and 1% of that to glucose, respectively, which was consistent with the results in the literature.[40]

4. Conclusions

In summary, a three-dimensionally ordered freestanding porous platinum nanowire array electrode integrating a porous nanostructure and a well-organized nanowire array was simply fabricated by co-electrodeposition and de-alloying strategies. PPNWAE showed high electrochemical activity, fast mass transport and effective enzyme utilization due to its larger specific surface area and rougher surface structure. The PPNWAE/GOD glucose biosensor performed in a fairly wide detection range by boosting the upper detection limit to 189.5 mM, and presented a relatively small Michaelis–Menten constant k_m, indicating the preservation of GOD bioactivity on PPNWAE. Compared with PNWAE, PPNWAE had enhanced GOD activity and provided a superior performance, such as a lower detection limit, higher sensitivity and smaller k_m value. In

Table 2 Comparison of the performance of the present sensor and some electrochemical glucose biosensors

Biosensor[a]	Sensitivity/μA cm^{-2} mM^{-1}	Detection limit/μM	Detection range/mM	Ref.
Pt–Pb NWAE	11.25	8	0.008–11	17
MPP	9.6	—	−10	21
GCE/PtNW-CNT-CHIT/GOD	30	3	0.005–15	34
GNTE/GOD	8.77	100	0.4–11	40
AuE/MWCNTs-BA/GOD	23.5	10	0.01–2.5	43
NPG	20.1	3	1–18	44
GCE/CHIT-GNW/GOD	—	5	0.01–20	45
PNWAE/GOD	4.21	83.3	0.083–182	This work
PPNWAE/GOD	8.74	4.5	0.0045–189.5	This work

[a] NWAE: nanowire array electrode, MPP: mesoporous platinum, GCE: glassy carbon electrode, PtNW: platinum nanowire, CNT: carbon nantube, CHIT: chitosan, GOD: glucose oxidase, GNTE: gold nanotubes electrode, AuE: gold electrode, MWCNTs: multi-walled carbon nanotubes, BA: 1-one-butyric acid, NPG: nanoporous gold, GNW: gold nanowires.

particular, the fabrication strategy could be extended to other noble metal and alloy electrodes. The present results suggested PPNWAE with the special structure reported here may offer a promising platform for various biosensing and bioelectronics applications.

Acknowledgements

We acknowledge financial support from the Nation Natural Science of China (51072217), Excellent Academic Leaders Plan of Shanghai (Y15SX81801), and Director's Initiative Fund of State Key Laboratory of High Performance Ceramics and Superfine Microstructure.

References

1 L. C. Clark and C. Lyons, *Ann. N. Y. Acad. Sci.*, 2006, **102**, 29–45.
2 J. S. Ye, Y. Wen, W. D. Zhang, L. M. Gan, G. Q. Xu and F. S. Sheu, *Electrochem. Commun.*, 2004, **6**, 66–70.
3 L. D. Zhu, Y. X. Li, F. M. Tian, B. Xu and G. Y. Zhu, *Sens. Actuators, B*, 2002, **84**, 265–270.
4 K. E. Shafer-Peltier, C. L. Haynes, M. R. Glucksberg and R. P. Van Duyne, *J. Am. Chem. Soc.*, 2003, **125**, 588–593.
5 D. Lee, J. Lee, J. Kim, H. B. Na, B. Kim, C. H. Shin, J. H. Kwak, A. Dohnalkova, J. W. Grate, T. Hyeon and H. S. Kim, *Adv. Mater.*, 2005, **17**, 2828–2833.
6 X. L. Luo, J. J. Xu, Y. Du and H. Y. Chen, *Anal. Biochem.*, 2004, **334**, 284–289.
7 W. Zhao, J. J. Xu, C. G. Shi and H. Y. Chen, *Langmuir*, 2005, **21**, 9630–9634.
8 S. H. Lim, J. Wei, J. Y. Lin, Q. T. Li and J. K. You, *Biosens. Bioelectron.*, 2005, **20**, 2341–2346.
9 J. M. Kim, H. I. Joh, S. M. Jo, D. J. Ahn, H. Y. Ha, S. A. Hong and S. K. Kim, *Electrochim. Acta*, 2010, **55**, 4827–4835.
10 M. De Leo, A. Kuhn and P. Ugo, *Electroanalysis*, 2007, **19**, 227–236.
11 H. W. Liang, X. A. Cao, F. Zhou, C. H. Cui, W. J. Zhang and S. H. Yu, *Adv. Mater.*, 2011, **23**, 1467–1471.
12 J. H. Yuan, K. Wang and X. H. Xia, *Adv. Funct. Mater.*, 2005, **15**, 803–809.
13 Y. G. Guo, J. S. Hu, H. M. Zhang, H. P. Liang, L. J. Wan and C. L. Bai, *Adv. Mater.*, 2005, **17**, 746–750.
14 A. Uhlig, U. Schnakemberg and R. Hintsche, *Electroanalysis*, 1997, **9**, 125–129.
15 S. M. Radke and E. C. Alocilja, *Biosens. Bioelectron.*, 2005, **20**, 1662–1667.
16 R. H. Petrucci, W. S. Harwood and G. E. Herring, *General Chemistry: Principles & Modern Applications*, Prentice Hall, Toronto, 9th edn, 2007, p. 606.
17 Y. Bai, Y. Sun and C. Sun, *Biosens. Bioelectron.*, 2008, **24**, 579–585.
18 M. Jamal, J. Xu and K. M. Razeeb, *Biosens. Bioelectron.*, 2010, **26**, 1420–1424.
19 F. X. Zhong, R. L. Zong and Y. F. Zhu, *J. Nanosci. Nanotechnol.*, 2009, **9**, 2437–2441.
20 S. B. Hall, E. A. Khudaish and A. L. Hart, *Electrochim. Acta*, 2000, **45**, 3573–3579.
21 S. Park, T. D. Chung and H. C. Kim, *Anal. Chem.*, 2003, **75**, 3046–3049.
22 S. A. G. Evans, J. M. Elliott, L. M. Andrews, P. N. Bartlett, P. J. Doyle and G. Denuault, *Anal. Chem.*, 2002, **74**, 1322–1326.
23 X. Y. Zhang, W. Lu, J. Y. Da, H. T. Wang, D. Y. Zhao and P. A. Webley, *Chem. Commun.*, 2009, 195–197.
24 A. J. Forty, *Nature*, 1979, **282**, 597–598.
25 Y. Y. Liu, Y. C. Zhu, Y. Zeng and F. F. Xu, *Nanoscale Res. Lett.*, 2009, **4**, 210–215.
26 Y. J. Song, S. B. Han and K. W. Park, *Mater. Lett.*, 2010, **64**, 1981–1984.
27 M. N. Qu, G. Y. Zhao, Q. Wang, X. P. Cao and J. Y. Zhang, *Nanotechnology*, 2008, **19**, 055707.
28 G. Y. Zhao, C. L. Xu, D. J. Guo, H. Li and H. L. Li, *Appl. Surf. Sci.*, 2007, **253**, 3242–3246.
29 Y. H. Lin, F. Lu, Y. Tu and Z. F. Ren, *Nano Lett.*, 2004, **4**, 191–195.
30 D. T. Sawyer, A. Sobkowiak and J. L. Roberts, *Electrochemistry for Chemists*, Wiley, New York, 2nd edn, 1995, p. 216.
31 Y. S. Lu, M. H. Yang, F. L. Qu, G. L. Shen and R. Q. Yu, *Anal. Lett.*, 2007, **40**, 875–886.
32 L. Qian and X. R. Yang, *Talanta*, 2006, **68**, 721–727.
33 M. H. Yang, F. L. Qu, Y. S. Lu, Y. He, G. L. Shen and R. Q. Yu, *Biomaterials*, 2006, **27**, 5944–5950.
34 F. L. Qu, M. H. Yang, G. L. Shen and R. Q. Yu, *Biosens. Bioelectron.*, 2007, **22**, 1749–1755.
35 X. Chen, J. J. Zhang, J. Xuan and J. J. Zhu, *Nano Res.*, 2009, **2**, 210–219.
36 A. Norlin, J. Pan and C. Leygraf, *Biomol. Eng.*, 2002, **19**, 67–71.
37 S. J. Ding, B. W. Chang, C. C. Wu, M. F. Lai and H. C. Chang, *Electrochim. Acta*, 2005, **50**, 3660–3666.
38 J. B. Jorcin, M. E. Orazem, N. Pebere and B. Tribollet, *Electrochim. Acta*, 2006, **51**, 1473–1479.
39 Q. C. Ruan, Y. C. Zhu, F. Li, J. W. Xiao, Y. Zeng and F. F. Xu, *J. Colloid Interface Sci.*, 2009, **333**, 725–733.
40 Y. L. Wang, Y. C. Zhu, Y. Y. Liu, Y. Yang, Q. C. Ruan and F. F. Xu, *J. Nanosci. Nanotechnol.*, 2010, **10**, 8286–8292.
41 A. J. Bard and L. R. Faulkner, *Electrochemical Methods: Fundamentals and Applications*, Wiley, New York, 2nd edn, 2000, p. 544.
42 J. N. Xie, S. Wang, L. Aryasomayajula and V. K. Varadan, *Nanotechnology*, 2007, **18**, 065503.
43 M. Y. Hua, Y. C. Lin, R. Y. Tsai and H. C. Chen, *J. Mater. Chem.*, 2012, **22**, 2566–2574.
44 L. Y. Chen, X. Y. Lang, T. Fujita and M. W. Chen, *Scr. Mater.*, 2011, **65**, 17–20.
45 Y. H. Lu, M. H. Yang, F. L. Qu, G. L. Shen and R. Q. Yu, *Bioelectrochemistry*, 2007, **71**, 211–216.
46 A. Kicela and S. Daniele, *Talanta*, 2006, **68**, 1632–1639.
47 M. D. Shirsat, C. O. Too and G. G. Wallace, *Electroanalysis*, 2008, **20**, 150–156.
48 F. R. Shu and G. S. Wilson, *Anal. Chem.*, 1976, **48**, 1679–1686.
49 X. Chen, J. Jia and S. Dong, *Electroanalysis*, 2003, **15**, 608–612.
50 Z. W. Zhao, X. J. Chen, B. K. Tay, J. S. Chen, Z. J. Han and K. A. Khor, *Biosens. Bioelectron.*, 2007, **23**, 135–139.
51 D. Shan, M. Zhu, H. Xue and S. Cosnier, *Biosens. Bioelectron.*, 2007, **22**, 1612–1617.
52 Y. M. Uang and T. C. Chou, *Biosens. Bioelectron.*, 2003, **19**, 141–147.
53 S. Su, Y. He, S. Song, D. Li, L. Wang, C. Fan and S. T. Lee, *Nanoscale*, 2010, **2**, 1704–1707.
54 H. J. Hecht, D. Schomburg, H. Kalisz and R. D. Schmid, *Biosens. Bioelectron.*, 1993, **8**, 197–203.
55 D. E. Koshland, *Proc. Natl. Acad. Sci. U. S. A.*, 1958, **44**, 98–104.